EUROPEAN JOURNAL OF MATERIALS SCIENCE AND ENGINEERING
Volume 10, Issue 3, 2025: 181-194 | www.ejmse.ro | ISSN: 2537-4338

EJMSE

DOI: 10.36868/ejmse.2025.10.03.181

DFT FUKUI DESCRIPTOR-BASED PREDICTION OF ARSENIC ADSORPTION ON GRAPHENE

Olusola Ibraheem AYENI[1,2][0009-0001-5483-2422], Toyese OYEGOKE[1,2*][0000-0002-2026-6864]

[1] CAD-Engineering of Processes and Reactive Materials Group, Chemical Engineering Department, Faculty of Engineering, Ahmadu Bello University, Zaria, Nigeria.
[2] Green Science Forum - Modeling & Simulation, Pencil Team, Ahmadu Bello University, Zaria, Nigeria.

Abstract

Arsenic contamination in water remains a significant environmental and public health challenge, necessitating efficient removal strategies. This study employs advanced quantum mechanical calculations to quantitatively evaluate arsenic's interactions with graphene and water under vacuum and aqueous conditions. Key molecular descriptors, including electron affinity (EA) and global electrophilicity index (GEI), reveal that water (EA = -1.85 eV, GEI = 0.94 eV) and graphene (EA = 1.34 eV, GEI = 2.81 eV) exhibit a higher electron-donating capacity, while arsenic demonstrates strong electron-accepting (EA = 4.87 eV) and electrophilic behavior (GEI = 39.19 eV). These findings suggest that arsenic, being highly electrophilic, preferentially adsorbs onto electron-rich materials like graphene, which has significantly lower GEI and EA values. Additionally, interaction energy gap calculations indicate that arsenic interacts more strongly with graphene (IEGAE = 0.61 eV) than with water (IEGAE = 3.05 eV), reinforcing graphene's superior adsorption efficiency. A similar trend is observed in the aqueous environment, with a slight reduction in interaction strength due to increased water molecule presence. Molecular orbital analyses, including electrostatic potential mapping and interaction energy band gaps, further confirm graphene's superior affinity for arsenic removal. These insights highlight graphene's potential as an advanced adsorbent, offering a sustainable solution for arsenic mitigation in water treatment applications.

Keywords: *heavy metal, modeling, simulation, adsorption, 2D materials, graphene, arsenic, environment.*

Introduction

Arsenic contamination in water and the atmosphere has emerged as a pressing environmental and public health issue due to its toxic effects on both human populations and aquatic ecosystems [1,2]. Arsenic, particularly in its inorganic forms, has been classified as a Group 1 carcinogen by the International Agency for Research on Cancer (IARC), with long-term exposure linked to various forms of cancer, cardiovascular diseases, and developmental disorders [3–5]. This pollutant primarily originates from industrial activities such as mining, smelting, and the use of arsenic-laden pesticides, where wastewater containing arsenic is often released into the environment without adequate treatment [6–8]. As a result, there is an increasing global demand for effective and sustainable methods to mitigate arsenic contamination, particularly in water, where it poses the most significant risk.

Traditional methods of arsenic removal, such as chemical precipitation, ion exchange, and adsorption using activated carbon, have shown limited efficiency, high costs, or operational challenges, particularly in developing regions [6,8–12]. Kanel et al. [8] reiterated that various

*Corresponding author: oyegoketoyese@gmail.com

studies in the literature have employed different approaches for arsenic removal, with adsorption being one of the most common methods. The literature further indicates that adsorbents such as activated alumina [8], modified biochar [8,9], iron oxides [8], and modified clay [8,10,12] have been widely used, particularly for treating wastewater from geochemical processes. The use of polymeric aluminum and iron species for modifying montmorillonite clay, as reported in the literature [10], was confirmed to enhance its arsenic adsorption capacity. Additionally, Sarkar et al. [11] suggested that future research should focus on developing more efficient and cost-effective arsenic removal technologies while integrating geochemical insights to enhance performance and sustainability.

As a result, research has shifted toward the development of advanced materials capable of selectively and efficiently removing arsenic from water. Among these materials, graphene has gained significant attention due to its unique physicochemical properties, including high surface area, chemical stability, and exceptional electronic properties.

Recent studies [13–17] have demonstrated that graphene-based materials can adsorb various pollutants from wastewater and flue gas emissions, highlighting their potential for arsenic remediation. Aliyu et al. [13] confirmed the significant role of functionalized graphene in DNA sequencing applications. Oyegoke et al. [14] and Szczęśniak et al. [16] extended the study of graphene-based materials, reaffirming their suitability for the removal of hydrogen sulfide and other gases from gas stream. Rout et al. [15] and Lazar et al. [17] demonstrated graphene's effectiveness in adsorbing organic molecules such as acetone, acetonitrile, dichloromethane, ethanol, ethyl acetate, hexane, and toluene. Notably, Lazar et al. [17] reported that adsorption enthalpies were primarily influenced by interaction energy, with toluene exhibiting the strongest adsorption strength and dichloromethane the weakest.

However, studies on the use of graphene-based materials for arsenic removal from wastewater, particularly from effluents released by geochemical exploration industries, remain limited. Among the few works that explored graphene-based material for arsenic removal includes, Galstenkova et al. [18] designed an improved graphene-based material by formulating a nanocomposite of iron oxide and reduced graphene oxide for arsenic removal. Their study further reiterated the significance of incorporating iron oxide into graphene oxide, demonstrating a sorption capacity of 8.90 mg/g. Hossain et al. [19] further revealed that enhancing the magnetic properties of graphene oxide significantly improves its sorption capacity, reaching 50.20 mg/g at room temperature. Similarly, studies such as Baskan & Hadimlioglu [20] and others [21–23] have also emphasized that the presence of iron oxide in the adsorbent material greatly enhances its sorption capacity. Rodríguez-Caicedo et al. [24]) conducted a study in Mexico and Colombia, demonstrating an arsenic adsorption capacity of 99.13 mg/g at 308 K under competitive conditions with other ions. Utilizing $NaNO_3$- and $KMnO_4$-oxidized graphene as an adsorbent, their findings exceeded the sorption capacity recorded in the study by Galstenkova et al. [18].

Despite the growing interest in graphene for arsenic removal, existing studies primarily focus on either computational predictions or experimental approaches without integrating a cost-effective and reliable quantum mechanical framework to elucidate the fundamental interactions at the molecular level. Furthermore, while some works have explored bonding interactions, there is limited research utilizing hybrid quantum mechanical methods, such as PM3/B3LYP-D3, to assess adsorption behavior using Fukui function-based descriptors. This gap in understanding the electronic properties, interaction energies, and adsorption potential of arsenic on graphene in both vacuum and aqueous environments hinders the precise tailoring of graphene-based materials for optimized pollutant removal. By addressing this, the present study provides a deeper theoretical insight into arsenic adsorption mechanisms, laying the groundwork for more efficient and sustainable water purification technologies.

However, understanding the fundamental interactions between arsenic and graphene is crucial to optimizing its performance for water purification. A hybrid quantum mechanical method, combining the use of density functional theory (B3LYP-D3) [25] with the semi-empirical method

(PM3) [26], provides a powerful tool for studying these interactions at the molecular level at an affordable cost [20]. These techniques offer critical insights into the electronic properties of both arsenic and graphene, including molecular orbital energies, electron affinities, ionization potentials, and interaction energies—factors essential for designing materials for targeted pollutant removal. Hence, this study explores the interaction potential between arsenic and graphene using a hybrid quantum mechanical (PM3/B3LYP-D3) approach, incorporating Fukui function-based molecular descriptors. Without directly modeling bonding formation, this preliminary study examines arsenic adsorption processes through interaction energy and band gap computations (based on ionization potential and electron affinity) in both vacuum and aqueous environments [27–30]. The findings provide valuable insights into the potential of graphene as an efficient material for arsenic removal, contributing to the advancement of sustainable environmental remediation strategies. Furthermore, the study reassesses its predictions against recent related studies [31] that have explored bonding interactions in the literature.

Computational Methodology

Using Spartan (a molecular modeling and computational chemistry-based simulation package), the chosen package developed by Wavefunction Inc. USA, we built various molecular structures needed for this study and carried out geometry and energy calculations for all of them. Based on the computed energies and molecular properties, this study looks at how graphene interacts with other substances in different environments, including both water and vacuum. This analysis helps us understand how these molecular interactions can lead to the adsorption of arsenic from wastewater.

Table 1 in this section provides relevant information employed in the study like the mathematical models and computational tools used in calculating the various molecular properties for the respective species considered in the study. Whereas, the later section of this report provides detailed information used in the structural geometry and energy calculations ran with the aid of the Spartan package.

Energy and Geometry Optimization

The molecules investigated in this study were constructed using Spartan Student v9.0.3 (Oct 27, 2022) on a Lenovo T495 laptop. The initial geometries were optimized using the PM3 method [26], with a convergence criterion of 1E-9 a.u. Subsequently, single-point energy calculations were performed using the B3LYP-D3 [25,33] method with a 6-31G* basis set on Spartan v24, applied in both vacuum and aqueous environments. This approach includes the Grimme D3 [34] dispersion correction to enhance the accuracy of density functional theory (DFT) calculations [25,32]. These later calculations were executed on a Dell Precision Mobile Workstation 3250, maintaining the same convergence criterion of 1E-5 a.u. under both vacuum and aqueous conditions.

Molecular Properties Calculations

In this section, we detail the molecular properties examined in this research, along with the relevant mathematical expressions, the calculation codes used in Spartan's spreadsheet, and their respective notations. To ensure accuracy and minimize human error, all calculations were conducted using Spartan’s built-in spreadsheet feature. The spreadsheet codes are derived from Spartan's output and are used for calculating electronic properties post-optimization. All molecular properties listed in Table 1 were calculated using the built-in spreadsheet feature of Spartan, ensuring accuracy and minimizing human error.

Table 1. Molecular Properties with their expression.

Molecular Properties' Description / Definition	Mathematical Expressions	Spartan Spreadsheet Calculation Code [32]
Highest Occupied Molecular Orbital Energy (EHOMO): Energy level of the highest occupied orbital in a molecule, indicating the molecule's ability to donate electrons.	EHOMO = E_{HOMO}	EHOMO (eV) = @HOMO*@hart2ev
Lowest Unoccupied Molecular Orbital Energy (ELUMO): Energy level of the lowest unoccupied orbital, representing the molecule's ability to accept electrons.	ELUMO = E_{LUMO}	ELUMO(eV)= @LUMO*@hart2ev
Ionization Potential (IP): Energy required to remove an electron from the HOMO.	IP = - E_{HOMO}	IP (eV) = -@HOMO* @hart2ev
Electron Affinity (EA): Energy released when an electron is added to the LUMO.	EA = - E_{LUMO}	EA (eV) = -@LUMO* @hart2ev
Electronegativity (EN): Tendency of an atom/molecule to attract electrons.	EN = (IP+EA)/2	EN (eV) = (-(@LUMO+ @HOMO)/2)*@hart2ev
Chemical Hardness (CH): Measure of resistance to change in electron distribution.	CH = (IP-EA)/2	CH (eV) = (((@LUMO- @HOMO)/2)*@hart2ev
Electronic Band Gap (Egap): Energy difference between the HOMO and LUMO, indicative of a molecule's reactivity.	Egap = IP – EA	Egap (eV) = (@LUMO-@HOMO) *@hart2ev
Global Electrophilicity Index (GEI): Index showing the molecule's ability to accept electrons.	GEI = (-IP - EA)/2)^2/ (IP – EA)	GEI (eV) = ((((@LUMO +@HOMO)/2)^2)/ (2*((@LUMO-@HOMO)/2)) *@hart2ev
Interaction Energy Gap using AS as IP (IEGAI): Measures the interaction between the adsorbate's IP and the system's EA; useful in evaluating donor-acceptor properties.	IEGAI = IP(AS)-EA	IEGAI (eV) = (- (@ref(@row("AS"),@HOMO))+ (@LUMO))*@hart2ev
Interaction Energy Gap using AS as EA (IEGAE): Measures the interaction between the system's IP and the adsorbate's EA.	IEGAE = IP-EA(AS)	IEGAE = (-(@HOMO) +(@ref(@row("AS"),@LUMO))) *@hart2ev
Interaction Energy Gap using Water as IP (IEGWI): Compares water's ionization potential with the EA of the system. Useful in aqueous interaction studies.	IEGWI = IP(H_20)-EA	IEGWI(eV)=(-(@ref(@row("H2O"), @HOMO))+(@LUMO))*@hart2ev
Interaction Energy Gap using Water as EA (IEGWE): Compares the system's IP with the electron affinity of water.	IEGWE = IP- EA (H_2O)	IEGWE = (-(@HOMO) +(@ref(@row ("H2O"), @LUMO)))*@hart2ev
Interaction Energy Gap using Graphene as IP (IEGGI): Interaction energy difference between graphene's IP and the system's EA. Relevant in surface interaction studies.	IEGGI = IP(GRA)-EA	IEGGI (eV) = (-(@ref(@row("coronene"), @HOMO))+(@LUMO))* @hart2ev
Interaction Energy Gap using Graphene as EA (IEGGE): Interaction gap between the system's IP and graphene's EA.	IEGWE = IP-EA(GRA)	IEGGE = (-(@HOMO) +(@ref(@row("coronene"),@LUMO)))*@hart 2ev

Results and discussions

Analysis of the Species' Molecular Properties

To enhance our understanding of the interaction between arsenic (the pollutant) and the graphene surface, this study evaluates various molecular properties in both vacuum and aqueous environments. The assessed properties, presented in Tables 2 and 3, include ionization potential (IP), highest occupied molecular orbital energy (EHOMO, accounts for the capability to donate electron), lowest unoccupied molecular orbital energy (ELUMO, defines the electrons acceptance capability), electron affinity (EA), energy gap (Egap), and interaction energy band gaps (IEGAI, IEGAE, IEGWI, IEGWE, IEGGI, and IEGGE as described in Table 1). Analysis of the data in Tables 2 and 3 indicates that while specific values vary between the vacuum and aqueous environments, the overall trends in molecular properties remain consistent across both conditions. The Ionization Potential (IP) evaluated as the negative of the HOMO energy, reflects a species' ability to ionize and release electrons to interacting species [35–37]. Water exhibited the strongest ionization potential, hence, has the most negative HOMO energy in Table 2 when compared to other interacting species in both environments.

Table 2. Molecular properties of the interacting species across different environment

Medium	Species	E HOMO (eV)	E LUMO (eV)	IP (eV)	EA (eV)	EN (eV)	CH (eV)	GEI (eV)	Egap (eV)
Vacuum	GRA	-5.49	-1.34	5.49	1.34	3.41	2.07	2.81	4.15
	AS	-5.57	-4.87	5.57	4.87	5.22	0.35	39.19	0.70
	H_20	-7.92	1.85	7.92	-1.85	3.04	4.89	0.94	9.77
Water	GRA	-5.58	-1.43	5.58	1.43	3.51	2.08	2.96	4.15
	AS	-5.62	-4.51	5.62	4.51	5.07	0.55	23.12	1.11
	H_2O	-7.95	2.43	7.95	-2.43	2.76	5.19	0.74	10.38

The Electron Affinity (EA) evaluated as the negative of the LUMO energy, reflects the ease with which a species accepts electrons [36–38]. The data in Table 2 reveals that As has a higher electron-accepting capability in both environments, this condition is observable in the analysis of their LUMO energy and GEI. In Table 2, As exceptional GEI value – a property which describes the ability of a molecule or atom to accept electron from nucleophiles, reveals that As has a better electrophilic character [37] and suggest that arsenic will preferably react with the graphene surface. This assertion is proven by further analysis into the interaction between the graphene surface and water.

The Energy Gap (Egap) represents the energy difference between the highest occupied molecular orbital (HOMO) and the lowest unoccupied molecular orbital (LUMO) in a molecule. A larger energy gap suggests greater stability, whereas a smaller gap indicates higher reactivity [37]. The data in Table 2 suggest that arsenic (As) interacts more readily with the reactive graphene in both environments (vacuum and water) compared to the more stable H_2O. Thus, implies that water would be less reactive compared to other species considered in the study, due to its high energy stability. This relationship between the energy gap and stability, as well as its inverse relationship with reactivity, is supported by Hamid et al. [39], Oyegoke [28], Lin et al. [40], Oyegoke & Adnan [41], and Huang et al. [42].

Additionally, analysis into the chemical hardness (CH) of the interacting species – a property that describes the reactivity of a material or resistance of a material to any changes in its electron density [43], or resistance of a material to charge transfer and change in electrons [44], which could result to either difficulty or ease in electron release [28]. The results in Table 2 reveals that water would be less reactive compared others species. Hence, graphene would potentially interact better with arsenic than water due to the lower value (0.35 eV) reported for arsenic. Table 2 shows that the hardness of a molecule is related to its Egap, the larger the energy band gap the harder the molecule and vice versa. [37,44].

Table 3. Interaction energy band gap for As, water, and graphene across different medium/environment

Medium/Environs	Species	IEGAI (eV)	IEGAE (eV)	IEGWI (eV)	IEGWE (eV)	IEGGI (eV)	IEGGE (eV)
Vacuum	GRA	4.23	0.61	6.58	7.34	4.15	4.15
	AS	0.70	0.70	3.05	7.42	0.61	4.23
	H2O	7.42	3.05	9.77	9.77	7.34	6.58
Water	GRA	4.19	1.07	6.52	8.01	4.15	4.15
	AS	1.11	1.11	3.44	8.04	1.07	4.19
	H2O	8.04	3.44	10.38	10.38	8.01	6.52

Further examination of the interaction energy band gap, using arsenic (As) as the ionization potential (IEGAI) and arsenic as the electron affinity (IEGAE), revealed that As prefers to accept electrons from the graphene surface rather than from water in both environments (Table 3), which agrees the literature [31] that seeks to modeling the chemical interaction or bonding of the species that confirms As to have shown preferential adsorption potential for the graphene surface over water, both in vacuum and aqueous system. Similarly, evaluating the interaction energy band gap of the graphene surface (IEGGI/IEGGE) indicates that graphene tends to donate electrons to As more readily than to water. The analysis of results (IEHAI through IEGGE) in Table 3 predicts a favorable interaction potential of As with the graphene surface.

Analysis of Interactive Sites

In this section, analyses into the HOMO, LUMO, and Electrostatic Map are presented (Table 4-9). The HOMO and LUMO maps provide insights into the molecular orbitals involved in electron donation and acceptance, respectively, indicating the reactivity sites on the individual specie surface [37]. The electrostatic map illustrates the charge distribution across the molecule, revealing potential interaction points and the overall polarity of the system [36]. DFT enables the determination of molecular quantities characterizing reactivity, shape and binding properties of molecules [37].

Analysis of Interactive Sites in Vacuum System

In this section, we analyze the molecular orbitals and electrostatic potential of the system. This includes examining the Highest Occupied Molecular Orbital (HOMO), Lowest Unoccupied Molecular Orbital (LUMO), and the electrostatic potential map, offering insights into the electronic structure and reactivity of the molecules in a vacuum environment. The HOMO surface represents the region of the molecule where the electron density is highest in the highest occupied molecular orbital, hence, this orbital tends to give its electron[37]. The HOMO surface in our analysis predicts that the electron density is predominantly localized at the edge (C-C site) of the graphene molecule, evenly distributed on the arsenic atom and at the oxygen site of the H_2O molecule (as shown in Table 4). Electron density increases in the order red < orange < yellow < green < blue.

The LUMO surface depicts the region where the molecule can accept electrons, representing the lowest unoccupied molecular orbital, hence, can be thought as the innermost orbital containing free places to accept electrons [37]. As observed in our vacuum system analysis (Table 5), this region is visible around the edge on the C-C site on the graphene, distributed at the lateral ends of the arsenic atom, and on the hydrogen site of the water molecule. Understanding these regions helps in predicting the molecule's behavior as an electrophile and its interaction with nucleophiles. As depicted on the legend, electron density increases down the colors.

Table 4. HOMO Map of the interacting species in vacuum system

	Graphene	As	H_2O
1st View	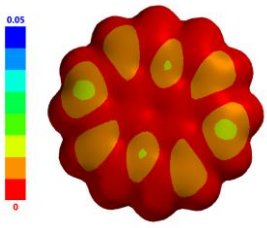	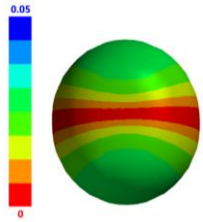	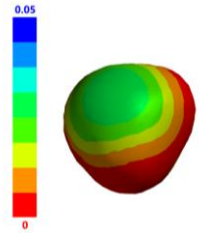
2nd View	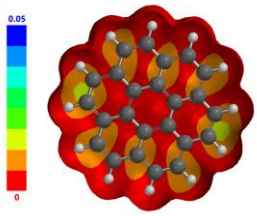	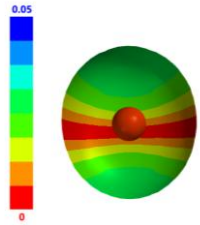	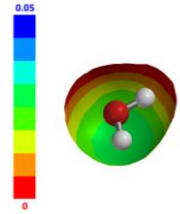

Table 5. LUMO Map of the interacting species in vacuum system.

	Graphene	As	H_2O
1st View	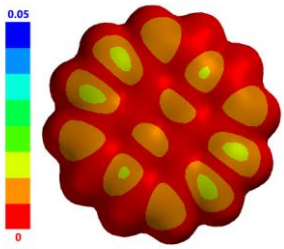	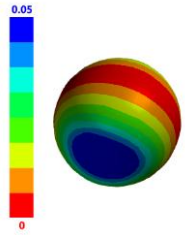	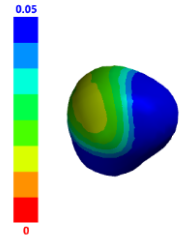
2nd View	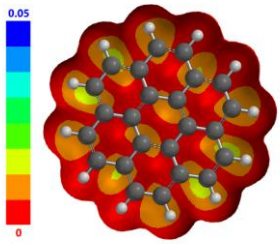	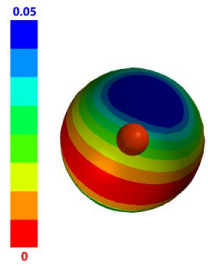	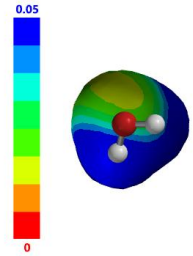

In our vacuum system analysis (Table 6), the electrostatic potential map reveals areas of the molecule that are electron-rich (negative potential) and electron-deficient (positive potential). Areas with negative potential suggests the likelihood of interacting with positively charged species and vice versa [45,46]. The graphene surface is distributed with mostly positive potential which supports its reactivity with arsenic, and the water molecule as reported on Table 2 and 3. These regions are indicative of the molecule's overall polarity and help in identifying sites for potential chemical interactions.

Table 6. Electrostatic Map of the interacting species in vacuum system.

	Graphene	As	H_2O
1st View	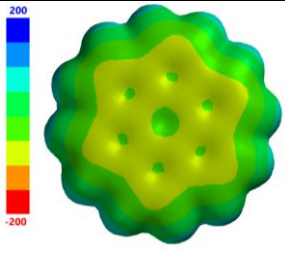	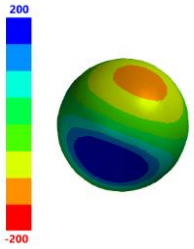	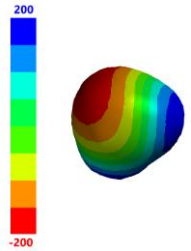
2nd View	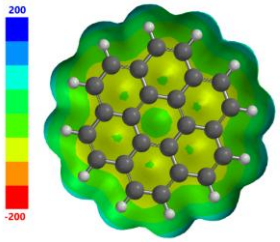	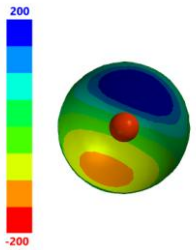	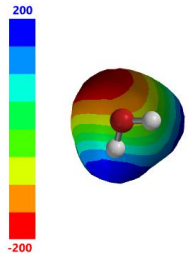

Analysis of Interactive Sites in Aqueous (Water) System

In this section, we present an analysis of the molecular orbitals and electrostatic potential of the system. These analyses, which include the Highest Occupied Molecular Orbital (HOMO), Lowest Unoccupied Molecular Orbital (LUMO), and the electrostatic potential map in Table 7 to 9, offer valuable insights into the electronic structure and reactivity of the molecules in an aqueous environment.

Moreover, the highest intensity sites on the HOMO map were identified as the arsenic (As) atom, the oxygen (O) site on water, and the carbon sites on the graphene sheet. These sites exhibited the most active HOMO regions, as indicated by their higher coloration in the HOMO map legend (Table 7). The analysis of the LUMO maps in Table 8 further reveals that arsenic (As) and the oxygen (O) site on the water molecule exhibit higher LUMO energy levels, as reflected by the intense blue coloration. In contrast, the carbon (C) site on the graphene sheet shows a lower LUMO energy rating.

A simultaneous examination of the HOMO and LUMO maps (Tables 7 and 8) suggests that water and arsenic (As) are more likely to act as electron acceptors when interacting with other species, such as graphene, due to their higher LUMO intensity. Conversely, graphene is expected to interact with arsenic (As) primarily as an electron donor rather than an acceptor, given its lower LUMO energy. These findings align with the molecular properties analyzed across different environments in this study (Tables 2 and 3) and with literature reports [27–29], which indicate that species with high ELUMO, EA, and GEI (using Fukui-based descriptors) tend to be electrophilic, while those with lower values act as electron donors.

Table 7. HOMO Map of the interacting species in aqueous system.

	Graphene	As	H_2O
1st View	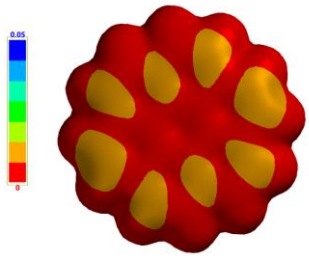	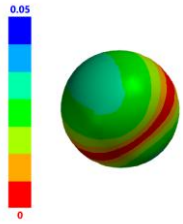	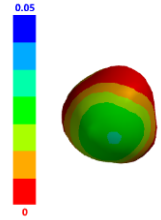
2nd View	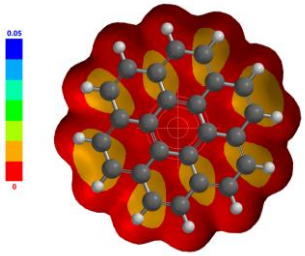	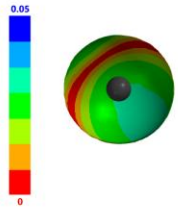	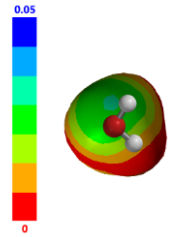

Table 8. LUMO Map of the interacting species in aqueous system.

	Graphene	As	H_2O
1st View	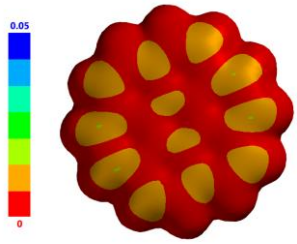	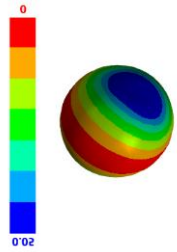	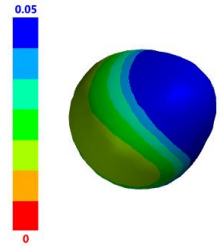
2nd View	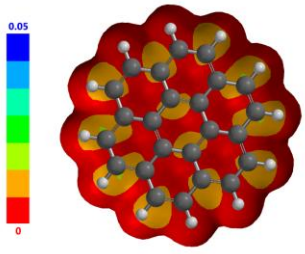	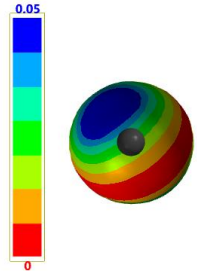	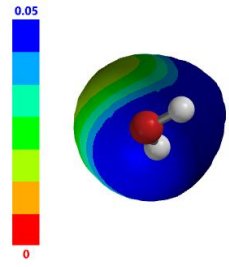

Table 9. Electrostatic Map of the interacting species in aqueous system.

	Graphene	As	H_2O
1st View	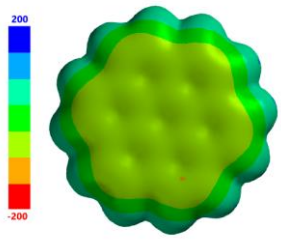	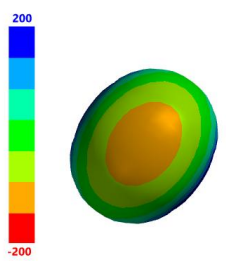	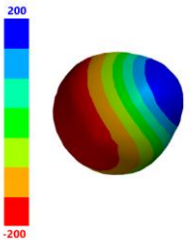
2nd View	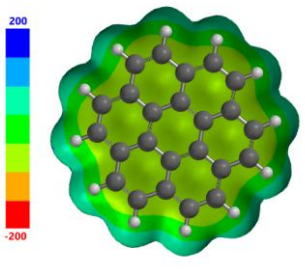	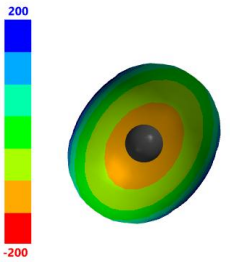	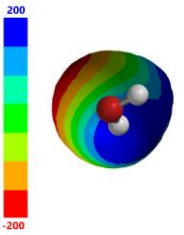

The slight differences observed in the surfaces reported for the HOMO, LUMO, and electrostatic potential maps are attributed to solvation effects. However, the interpretation of these surfaces remains consistent with the analyses conducted in the vacuum environment (Tables 5 to 7). This suggests that the results obtained in the vacuum case can reasonably predict the effects of solvation.

Conclusions

This study investigates the molecular properties of arsenic (As) and its interactions with graphene and water in both vacuum and aqueous environments. The findings confirm that arsenic exhibits a strong electron-accepting ability, with an electron affinity (EA) of 4.87 eV in vacuum and 4.51 eV in water, while water possesses a higher electron-donating capacity, with higher ionization potential (IP = 7.92 eV in vacuum and 7.95 eV in water) and negative EA values of -1.85 eV in vacuum and -2.43 eV in water. These trends remain consistent across different environmental conditions, reinforcing the fundamental electronic behavior of the studied species.

Further analyses of interaction energy and the global electrophilicity index (GEI) reveal that arsenic has a stronger affinity for graphene than for water. Arsenic's GEI is significantly higher (39.19 eV in vacuum and 23.12 eV in water) compared to graphene (2.81 eV in vacuum and 2.96 eV in water), indicating its high susceptibility to interaction with electron-rich surfaces. The lower interaction energy gap of arsenic with graphene (0.61 eV) compared to water (3.05 eV) suggests a more favorable adsorption process, making graphene a highly promising material for arsenic remediation.

Molecular orbital analysis, including the evaluation of HOMO-LUMO interactions, supports these findings by demonstrating that graphene's electronic structure facilitates stronger arsenic adsorption. The energy gap (Egap) of arsenic is significantly lower (0.70 eV in vacuum and 1.11 eV in water) than that of water (9.77 eV in vacuum and 10.38 eV in water), reinforcing arsenic's high reactivity. The results align with existing literature on adsorption modeling and confirm the reliability of molecular descriptors in predicting adsorption behavior. Additionally, the study highlights the significance of using quantum mechanical calculations for screening adsorbent

materials. The predictive power of DFT-based molecular descriptors offers a valuable preliminary tool for evaluating adsorption efficiency before conducting experimental studies.

Ultimately, this research contributes to the development of sustainable arsenic removal strategies. By demonstrating graphene's superior adsorption potential, the study provides insights that could enhance future applications in water treatment and environmental management.

Future Directions and Limitations

This study provides critical insights into arsenic adsorption on graphene but is limited by its exclusive reliance on computational methods. Further work can extend the study to other heavy metal contaminants, exploring the applicability of graphene-based materials for water purification technologies through a combined approach of experimental and computational methods.

Acknowledgments

The authors wish to acknowledge the support of Wavefunction Inc US for providing a discounted license for Student Spartan v9 (student-version) and a free 2-years license for Spartan 24 (full-version), which were respectively used for semi-empirical calculation and dispersion corrected B3LYP calculations in the energy calculation. Thanks for the automatic language and grammatical check ran with the aid of artificial intelligence (AI) tools like Grammarly in the report.

References

[1] Tsuda T, Babazono A, Ogawa T, Hamada H, Mino Y, Aoyama H, Kurumatani N, Nagira T, Hotta N, Harada M, Inomata S. *Inorganic arsenic: A dangerous enigma for mankind.* **Appl Organomet Chem, 1992**, 6, pp. 309–22. https://doi.org/10.1002/AOC.590060403.

[2] Tchounwou PB, Centeno JA, Patlolla AK. *Arsenic toxicity, mutagenesis, and carcinogenesis - A health risk assessment and management approach*. **Mol Cell Biochem, 2004,** 255, pp. 47–55. https://doi.org/10.1023/B:MCBI.0000007260.32981.B9/METRICS.

[3] Moore MN. Environmental Health Impacts of Natural and Man-Made Chemicals. Oxford Research Encyclopedia of Environmental Science, Oxford University Press; 2019. https://doi.org/10.1093/ACREFORE/9780199389414.013.343.

[4] Roy JS, Chatterjee D, Das N, Giri AK. *Substantial evidences indicate that inorganic arsenic is a genotoxic carcinogen: A review*. **Toxicol Res, 2018,** 34, pp. 311–24. https://doi.org/10.5487/TR.2018.34.4.311.

[5] Bjørklund G, Tippairote T, Rahaman MS, Aaseth J. *Developmental toxicity of arsenic: a drift from the classical dose–response relationship*. **Arch Toxicol, 2020,** 94, pp. 67–75. https://doi.org/10.1007/S00204-019-02628-X.

[6] Qasem NAA, Mohammed RH, Lawal DU. *Removal of heavy metal ions from wastewater: a comprehensive and critical review.* **Npj Clean Water, 2021,** 4, pp. 1–15. https://doi.org/10.1038/s41545-021-00127-0.

[7] Zhuang F, Huang J, Li H, Peng X, Xia L, Zhou L, Zhang T, Liu Z, He Q, Luo F, Yin H, Meng D. *Biogeochemical behavior and pollution control of arsenic in mining areas: A review.* **Front Microbiol, 2023,** 14, pp. 1043024. https://doi.org/10.3389/FMICB.2023.1043024/BIBTEX.

[8] Kanel SR, Das TK, Varma RS, Kurwadkar S, Chakraborty S, Joshi TP, Bezbaruah AN, Nadagouda MN. *Arsenic Contamination in Groundwater: Geochemical Basis of Treatment Technologies*. **ACS Environmental Au, 2023,** 3, pp. 135–52. https://doi.org/10.1021/ACSENVIRONAU.2C00053/ASSET/IMAGES/LARGE/VG2C00053_0016.JPEG.

[9] Sun Y, Yu F, Han C, Houda C, Hao M, Wang Q. *Research Progress on Adsorption of Arsenic from Water by Modified Biochar and Its Mechanism: A Review*. **Water, 2022,** 14, pp. 1691. https://doi.org/10.3390/W14111691.

[10] Ren X, Zhang Z, Luo H, Hu B, Dang Z, Yang C, Li L. *Adsorption of arsenic on modified montmorillonite.* **Appl Clay Sci, 2014,** 97–98, pp. 17–23. https://doi.org/10.1016/J.CLAY.2014.05.028.

[11] Sarkar S, Blaney LM, Gupta A, Ghosh D, Sengupta AK. *Arsenic removal from groundwater and its safe containment in a rural environment: Validation of a sustainable approach.* **Environ Sci Technol, 2008,** 42, pp. 4268–4273. https://doi.org/10.1021/ES702556T.

[12] Genç-Fuhrman H, Tjell JC, McConchie D. *Adsorption of Arsenic from Water Using Activated Neutralized Red Mud*. **Environ Sci Technol, 2004,** 38, pp. 2428–2434. https://doi.org/10.1021/ES035207H.

[13] Aliyu A, Tayo BO, Oyegoke T, Anye VC. *Computational Insight into Graphene Functionalization for DNA Sequencing: A DFT Approach*. **Proceedings, 2024,** 105, pp.43. https://doi.org/10.3390/PROCEEDINGS2024105043.

[14] Oyegoke T, Aliyu A, Uzochuwu MI, Hassan Y. *Enhancing hydrogen sulphide removal efficiency: A DFT study on selected functionalized graphene-based materials.* **Carbon Trends, 2024,** 15, pp. 100362. https://doi.org/10.1016/J.CARTRE.2024.100362.

[15] Rout DR, Jena HM, Baigenzhenov O, Hosseini-Bandegharaei A. *Graphene-based materials for effective adsorption of organic and inorganic pollutants: A critical and comprehensive review.* **Science of The Total Environment, 2023,** 863, pp. 160871. https://doi.org/10.1016/J.SCITOTENV.2022.160871.

[16] Szczęśniak B, Choma J, Jaroniec M. *Gas adsorption properties of graphene-based materials.* **Adv Colloid Interface Sci, 2017,** 243, pp. 46–59. https://doi.org/10.1016/J.CIS.2017.03.007.

[17] Lazar P, Karlický F, Jurecka P, Kocman M, Otyepková E, Šafářová K, Otyepka M. *Adsorption of small organic molecules on graphene*. **J Am Chem Soc, 2013,** 135, pp. 6372–6377. https://doi.org/10.1021/JA403162R/SUPPL_FILE/JA403162R_SI_001.PDF.

[18] Galstenkova MR, Mukhortova YR, Pryadko AS, Botvin V V., Wagner D V., Sharonova AA, Surmeneva MA, Surmenev RA. *A fixed-bed-column study on arsenic removal from water using an in situ-synthesized nanocomposite of magnetite and reduced graphene oxide*. **Nano-Structures & Nano-Objects, 2025,** 41, pp. 101431. https://doi.org/10.1016/J.NANOSO.2025.101431.

[19] Hossain MS, Yasmin S, Kabir MH. *Cost-effective synthesis of magnetic graphene oxide nanocomposite from waste battery for the removal of arsenic from aqueous solutions: Adsorption mechanism with DFT calculation*. **Journal of Saudi Chemical Society, 2024,** 28, pp. 101873. https://doi.org/10.1016/J.JSCS.2024.101873.

[20] Bilici Baskan M, Hadimlioglu S. *Removal of arsenate using graphene oxide-iron modified clinoptilolite-based composites: adsorption kinetic and column study*. **J Anal Sci Technol, 2021,** 12, pp. 1–16. https://doi.org/10.1186/S40543-021-00274-6/FIGURES/11.

[21] Sherlala AIA, Raman AA, Bello MM. *Adsorption of arsenic from aqueous solution using magnetic graphene oxide.* **IOP Conf Ser Mater Sci Eng, 2017**, 210, pp. 012007. https://doi.org/10.1088/1757-899X/210/1/012007.

[22] Sengupta S, Pari A, Biswas L, Shit P, Bhattacharyya K, Chattopadhyay AP. *Adsorption of arsenic on graphene oxide, reduced graphene oxide, and their fe3o4 doped nanocomposites*. **Biointerface Res Appl Chem, 2022**, 12, pp. 6196–6210. https://doi.org/10.33263/BRIAC125.61966210.

[23] Sherlala AIA, Raman AAA, Bello MM, Buthiyappan A. *Adsorption of arsenic using chitosan magnetic graphene oxide nanocomposite*. **J Environ Manage, 2019,** 246, pp. 547–56. https://doi.org/10.1016/J.JENVMAN.2019.05.117.

[24] Rodríguez-Caicedo JP, Joya-Cárdenas DR, Gallegos-Muñoz A, Abraham-Juárez MR, Zapata-Torres M, Damián-Ascencio CE, Saldaña-Robles A. *Advanced graphene oxide synthesis for arsenic removal from groundwater in Mexico and Colombia.* **Results in Engineering, 2025,** 25, pp. 104189. https://doi.org/10.1016/J.RINENG.2025.104189.

[25] Goerigk L. **A Comprehensive Overview of the DFT-D3 London-Dispersion Correction. Non-Covalent Interactions in Quantum Chemistry and Physics: Theory and Applications, Elsevier**, 2017, pp. 195–219. https://doi.org/10.1016/B978-0-12-809835-6.00007-4.

[26] Wu YY, Zhao FQ, Ju XH. A *Comparison of the Accuracy of Semi-empirical PM3, PDDG and PM6 methods in Predicting Heats of Formation for Organic Compounds*. **J Mex Chem Soc, 2014,** 58, pp. 223–229. https://doi.org/10.29356/JMCS.V58I2.182.

[27] Bendjeddou A, Abbaz T, Gouasmia A, Villemin D. *Molecular Structure, HOMO-LUMO, MEP and Fukui Function Analysis of Some TTF-donor Substituted Molecules Using DFT (B3LYP) Calculations*. **Int Res J Pure Appl Chem, 2016,** 12, pp. 1–9. https://doi.org/10.9734/irjpac/2016/27066.

[28] Oyegoke T, Dabai FadimatuN, Adamu U, Baba YJ. *Quantum mechanics calculation of molybdenum and tungsten influence on the CrM-oxide catalyst acidity*. **Hittite Journal of Science & Engineering, 2020,** 7, pp. 297–311. https://doi.org/10.17350/HJSE19030000199.

[29] Pucci R, Angilella GGN. *Density functional theory, chemical reactivity, and the Fukui functions*. **Found Chem, 2022,** 24, pp. 59–71. https://doi.org/10.1007/S10698-022-09416-Z.

[30] Cerón ML, Gomez T, Calatayud M, Cárdenas C. *Computing the Fukui Function in Solid-State Chemistry: Application to Alkaline Earth Oxides Bulk and Surfaces*. **Journal of Physical Chemistry A, 2020,** 124, pp. 2826–33. https://doi.org/10.1021/ACS.JPCA.0C00950/SUPPL_FILE/JP0C00950_SI_002.ZIP.

[31] Ayeni OI, Oyegoke T. *Computational insights into graphene-based materials for arsenic removal from wastewater: a hybrid quantum mechanical study*. **Discover Water, 2024**, 4, pp. 103. https://doi.org/10.1007/S43832-024-00160-3.

[32] Hehre WJ. **A guide to molecular mechanics and quantum chemical calculations.** Wavefunction; 2003.

[33] Schröder H, Hühnert J, Schwabe T. *Evaluation of DFT-D3 dispersion corrections for various structural benchmark sets.* **Journal of Chemical Physics, 2017,** 146, pp. 044115. https://doi.org/10.1063/1.4974840/195922.

[34] Grimme S. *Density functional theory with London dispersion corrections*. **Wiley Interdiscip Rev Comput Mol Sci, 2011**, 1, pp. 211–228. https://doi.org/10.1002/WCMS.30.

[35] Shah E V., Roy DR. **Group III–V hexagonal pnictide clusters and their promise for graphene-like materials. Atomic Clusters with Unusual Structure, Bonding and Reactivity: Theoretical Approaches, Computational Assessment and Applications** 2023:139–55. https://doi.org/10.1016/B978-0-12-822943-9.00009-7.

[36] Parsaee Z, Mohammadi K, Ghahramaninezhad M, Hosseinzadeh B. *A novel nano-sized binuclear nickel(ii) Schiff base complex as a precursor for NiO nanoparticles: synthesis, characterization, DFT study and antibacterial activity.* **New Journal of Chemistry, 2016**, 40, pp. 10569–10583. https://doi.org/10.1039/C6NJ02642G.

[37] Bendjeddou A, Abbaz T, Gouasmia A, Villemin D. *Molecular Structure, HOMO-LUMO, MEP and Fukui Function Analysis of Some TTF-donor Substituted Molecules Using DFT (B3LYP) Calculations*. **Int Res J Pure Appl Chem, 2016**, 12, pp. 1–9. https://doi.org/10.9734/IRJPAC/2016/27066.

[38] Rehman F ur, Waqas M, Imran M, Ibrahim MAA, Iqbal J, Khera RA, Hadia NMA, Al-Saeedi SI, Shaban M. *Approach toward Low Energy Loss in Symmetrical Nonfullerene Acceptor Molecules Inspired by Insertion of Different π-Spacers for Developing Efficient*

Organic Solar Cells. **ACS Omega, 2023**, 8, pp. 43792–43812. https://doi.org/10.1021/ACSOMEGA.3C05665.

[39] Hamid A, Deswal N, Pal S, Roy RK. **Components of density functional reactivity theory-based stabilization energy: descriptors for thermodynamic and kinetic reactivity. Chemical Reactivity (Volume 2: Approaches and Applications)**, Elsevier; 2023, p. 181–226. https://doi.org/10.1016/B978-0-32-390259-5.00013-5.

[40] Lin CY, Marque SRA, Matyjaszewski K, Coote ML. *Linear-free energy relationships for modeling structure-reactivity trends in controlled radical polymerization*. **Macromolecules, 2011**, 44, pp. 7568–7583. https://doi.org/10.1021/MA2014996/SUPPL_FILE/MA2014996_SI_001.PDF.

[41] Oyegoke T, Adnan A. *Impact of Selected Adsorbent Functional Groups on Chromium Sorption Capacities In An Effluent Treatment: A DFT Study*. **The Journal of Engineering Research [TJER], 2024**, 21, pp. 59–70. https://doi.org/10.53540/TJER.VOL21ISS1PP59-70.

[42] Huang Y, Rong C, Zhang R, Liu S. *Evaluating frontier orbital energy and HOMO/LUMO gap with descriptors from density functional reactivity theory*. **J Mol Model, 2017,** 23, pp. 1–12. https://doi.org/10.1007/S00894-016-3175-X/METRICS.

[43] Miranda-Quintana RA, Heidar-Zadeh F, Fias S, Chapman AEA, Liu S, Morell C, Gómez T, Cárdenas C, Ayers PW. *Molecular interactions from the density functional theory for chemical reactivity: Interaction chemical potential, hardness, and reactivity principles*. **Front Chem, 2022**, 10, pp. 929464. https://doi.org/10.3389/FCHEM.2022.929464/BIBTEX.

[44] Gázquez JL. **Hardness and softness in density functional theory: Chemical Hardness**, Springer, Berlin, Heidelberg; 1993, p. 27–43. https://doi.org/10.1007/BFB0036798.

[45] Ogunwale GJ, Louis H, Unimuke TO, Mathias GE, Owen AE, Edet HO, Enudi OC, Oluwasanmi EO, Adeyinka AS, Doust Mohammadi M. *Interaction of 5-Fluorouracil on the Surfaces of Pristine and Functionalized Ca12O12 Nanocages: An Intuition from DFT*. **ACS Omega, 2023**, 8, pp. 13551–13568. https://doi.org/10.1021/ACSOMEGA.2C03635.

[46] Yadav P, Rana M, Chowdhury P. *DFT and MD simulation investigation of favipiravir as an emerging antiviral option against viral protease (3CLpro) of SARS-CoV-2*. **J Mol Struct, 2021**, pp. 1246. https://doi.org/10.1016/J.MOLSTRUC.2021.131253.

Received: April 02, 2025
Accepted: July 16, 2025